Follow us @BoneJointRes

Freely available online OPEN ACCESS

BJR

BONE BIOLOGY

3D mapping and classification of tibial plateau fractures

X. Yao,
K. Zhou,
B. Lv,
L. Wang,
J. Xie,
X. Fu,
J. Yuan,
Y. Zhang

From The Affiliated People's Hospital of Jiangsu University, Zhenjiang, China

Aims

Tibial plateau fractures (TPFs) are complex injuries around the knee caused by high- or low-energy trauma. In the present study, we aimed to define the distribution and frequency of TPF lines using a 3D mapping technique and analyze the rationalization of divisions employed by frequently used classifications.

Methods

In total, 759 adult patients with 766 affected knees were retrospectively reviewed. The TPF fragments on CT were multiplanar reconstructed, and virtually reduced to match a 3D model of the proximal tibia. 3D heat mapping was subsequently created by graphically superimposing all fracture lines onto a tibia template.

Results

The cohort included 405 (53.4%) cases with left knee injuries, 347 (45.7%) cases with right knee injuries, and seven (0.9%) cases with bilateral injuries. On mapping, the hot zones of the fracture lines were mainly concentrated around the anterior cruciate ligament insertion, posterior cruciate ligament insertion, and the inner part of the lateral condyle that extended to the junctional zone between Gerdy's tubercle and the tibial tubercle. Moreover, the cold zones were scattered in the posteromedial fragment, superior tibiofibular syndesmosis, Gerdy's tubercle, and tibial tubercle. TPFs with different Orthopaedic Trauma Association/AO Foundation (OTA/AO) subtypes showed peculiar characteristics.

Conclusion

TPFs occurred more frequently in the lateral and intermedial column than in the medial column. Fracture lines of tibial plateau occur frequently in the transition zone with marked changes in cortical thickness. According to 3D mapping, the four-column and nine-segment classification had a high degree of matching as compared to the frequently used classifications.

Cite this article: *Bone Joint Res* **2020;9(6):258–267.**

Keywords: Tibial plateau fracture, 3D mapping, Fracture classification

Article focus

- We present the distribution and frequency of fracture lines for 766 tibial plateau fractures (TPFs) using the 3D heat mapping technique.
- The rationality of several classifications could be discussed according to the 3D distribution of fracture lines.

Key messages

- The distribution of fracture lines was not only dependent on the injury energy or mechanism, but was also distinctly related to the anatomical features of the proximal tibial area.
- The newly proposed intermedial column in four-column and nine-segment classification without cartilage coverage should be taken seriously.

Strengths and limitations

- The primary limitation is that the injury mechanism and the displacement of fragments of TPFs were neglected due to the virtual reduction procedure.
- This is the first time that the fracture lines of massive TPFs (more than 700) have been delineated in detail.

Correspondence should be sent to Yingqi Zhang; email: realzyq@163.com

doi: 10.1302/2046-3758.96.BJR-2019-0382.R2

Bone Joint Res 2020;9(6):258–267.

Introduction

Tibial plateau fractures (TPFs) are complex injuries around the knee caused by high- or low-energy trauma. The treatment strategy for TPF is often unclear due to the various possible fracture patterns and unsatisfactory outcomes.[1-3] A better understanding of the fracture line distribution and morphological features of major fragment is vital for therapeutic decision-making.[4] Fracture classification, including a simplified summary and fracture mapping, can help surgeons better comprehend, document, and communicate information about fractures. Based on plain radiography, early-stage classification systems (Hohl and Moore, Schatzker 1974, Orthopaedic Trauma Association/AO Foundation (OTA/AO) 2007) have played a crucial role in guiding surgical treatment during the past decades.[5-8] Due to the limitations of the technology, 2D classifications have apparent disadvantages in the identification and detailing of posterior fragments. With the advent of CT, novel classifications facilitated the understanding of TPF via a 3D approach. Luo et al[9] proposed the three-column (medial, lateral, and posterior columns) concept (Luo classification), whereas Chang et al[10] divided the upper surface into four quadrants.[9-11] Other systems proposed the precise division of tibial plateau into eight, ten, or nine segments.[12-14] Furthermore, the frequently used OTA/AO and Schatzker classifications added the axial plane subtypes in 2018.[15,16]

In addition, Yao et al[17] established a CT-based 'four-column and nine-segment' classification (Yao classification), and proposed a new intermedial column concept (containing the tubercle area, bare area, and anterior/posterior cruciate ligament (ACL/PCL) insertion area).[17] This new classification covered the entire bony structure of the proximal calves, highlighted the crucial ligament insertion, and enabled the clear definition of injury types for each column/segment. Although the Yao classification appears to be the most detailed system thus far, we believe that the fracture line distribution can be described more precisely and visually.

Traditional classifications describe the fracture characteristics in a rough and abstract manner using text documentation. In contrast, the heat mapping technique can clearly and intuitively indicate the distribution and frequency of fracture lines. This imaging technique has been newly developed, and is being widely used in irregular bone or the ends of long bone.[18-20] Molenaars et al[21] and Chen et al[22] have described the single axial mapping of the tibial plateau articular surface.[21,22] However, uniplanar mapping cannot reveal extra-articular fracture line distribution - a crucial aspect for plate positioning. Superior 3D fracture line heat mapping, including steric distribution information, can facilitate decision-making with regard to the surgical approach and fixation scheme.[23]

In the present study, we aimed to define the distribution and frequency of TPF fracture lines using the 3D heat mapping technique. We hypothesized that the fracture patterns and fracture line distribution are consistent in cases of TPF. Moreover, we sought to analyze the rationalization of divisions employed by frequently used classifications based on mapping.

Methods

Subjects. Between December 2007 and September 2018, a total of 825 adult patients with closed fracture of the proximal tibia at the Affiliated People's Hospital of Jiangsu University, Zhenjiang, China were enrolled. Patients with isolated avulsion fractures of the ACL/PCL and patellar ligament (PL) were included, whereas 41 cases with insufficient CT information were excluded. Additional exclusion criteria included cutting, club violence, bullet wounds, bone defects, periprosthetic fractures, and pathological fractures, as well as congenital or acquired malformation of the tibial plateau. In summary, a total of 759 patients (411 males and 348 females) with 766 affected knees were included in the cohort. The mean age of these patients was 51.5 years (SD 12.9). All fractures were identified using the OTA/AO and Yao classifications. This retrospective study has been approved by the ethical committee of the Affiliated People's Hospital of Jiangsu University.

Radiological analysis. TPF patients underwent CT scanning using a Siemens spiral CT scanner (Siemens, Berlin, Germany) after injury, and raw images (1.0 mm thick slices) were transferred into Mimics 17.0 software (Materialise, Leuven, Belgium).

Fracture mapping. TPF fragments were multiplanar reconstructed in Mimics and were virtually reduced. Data were subsequently exported into the 3-matic 10.0 software (Materialise), and the reconstructed fragments were rotated, normalized, and horizontally flipped, if necessary, to best match a 3D model of the proximal tibia. Smooth curves were delineated precisely on the template surface to reproduce the fracture line distribution of each TPF in 3-matic. The graphical superimposition of all fracture lines was transferred to E-3D software (Central South University, Changsha, China) and transformed into stereo fracture maps (Figure 1). 3D heat maps indicated the relative frequency of fracture lines using colours (blue to red: low to high incidence).

Data analysis. Qualitative data are shown as the number (percentage) and quantitative data are expressed as the mean (SD) using SPSS v19 (IBM, Armonk, New York, USA). Analysis of fracture line mapping was descriptive.

Results

The patient characteristics and radiological classification of the TPF are summarized in Tables I and II . A total of 759 patients with 766 injured knees were included (348 women, 411 men), including 405 (53.4%) left knee injuries, 347 (45.7%) right knee injuries, and seven (0.9%) cases with bilateral injuries. Among the 759 patients, the mean age was 51.5 years (SD 12.9) and fractures are most likely to occur among patients aged 50 to 59 years (Figure 2).

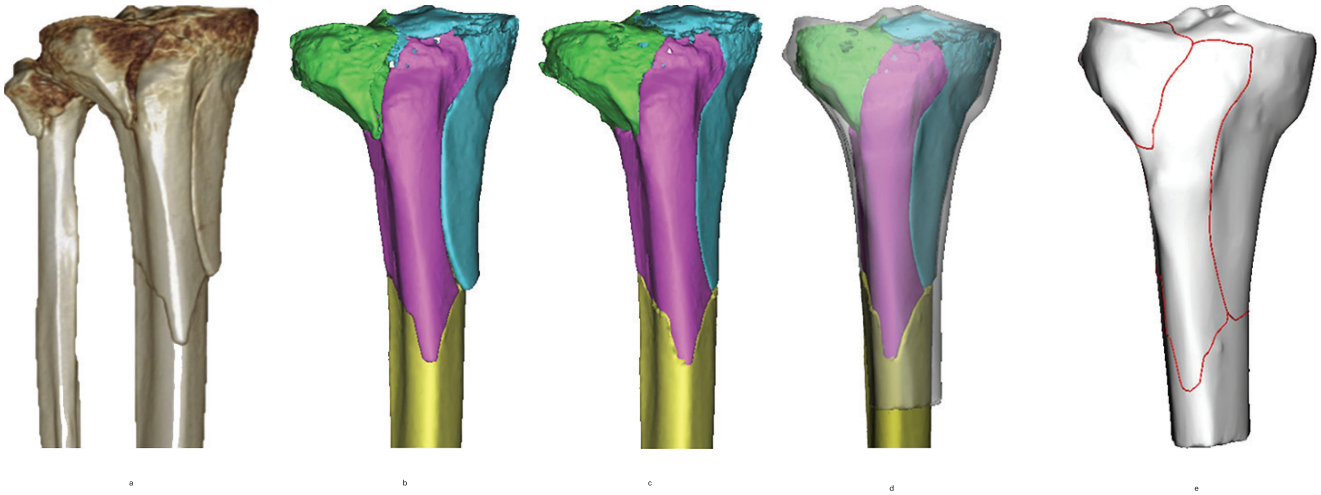

Fig. 1

The method used for the mapping of tibial plateau. a) 3D image of tibial plateau fracture in CT scans. b) Major fragments were reconstructed in Mimics (Materialise, Leuven, Belgium). c) Virtual reduction. d) Reduced fragments were adjusted to match the template in 3-matic 10.0 software (Materialise). e) Fracture lines were delineated on the template.

Table I. Patient demographics.

Demographic	Data (n = 759)
Mean age, yrs (SD)	
Male	49.7 (12.3)
Female	53.7 (13.4)
Total	51.5 (12.9)
Sex, n (%)	
Male	411 (54.2)
Female	348 (46.8)
Total	759 (100.0)
Knees, n (%)	
Left only	405 (53.4)
Right only	347 (45.7)
Bilateral	7 (0.9)
Total	759 (100.0)
OTA/AO classification, n (%)	
41.A	114 (14.9)
41.B	376 (49.1)
41 .C	276 (36.0)
Total	766 (100.0)

OTA/AO, Orthopaedic Trauma Association/AO Foundation.

Table II. Fracture characteristics according to the four-column and nine-segment classification.

Characteristic	Data, n (%)
Four columns	
Medial, n	238 (31.1)
Intermedial, n	574 (74.9)
Lateral, n	612 (79.9)
Fibular, n	237 (30.9)
Total	766 (100.0)
Nine segments	
a) anteromedial segment	167 (21.8)
b) posteromedial segment	177 (23.1)
c) tubercle segment	91 (11.9)
d) bare area	304 (39.7)
e) median segment	358 (46.7)
f) posteromedian segment	399 (52.1)
g) anterolateral segment	482 (62.9)
h) posterolateral segment	486 (63.4)
i) fibular segment	237 (30.9)
Total	766 (100.0)

The OTA/AO classification of the cohort was as follows: type A, 114 (14.9%); type B, 376 (49.1%); and type C, 276 (36.0%). According to the Yao classification, the most frequently affected columns included the lateral column (612, 79.9%) and intermedial column (574, 74.9%), and the less frequently involved columns included the medial column (238, 31.1%) and fibular column (237, 30.9%). The most frequently affected segments included the posterolateral (486, 63.4%), anterolateral (482, 62.9%), and posteromedian segments (399, 52.1%). The least frequently involved segment was the tubercle segment (91, 11.9%).

3D mapping. All the 766 fracture lines were aggregated on a tibia template (Figures 3a to 3e). On 3D heat mapping (Figures 3g to 3j; Supplementary Video 1), the hot zones were mainly concentrated around the ACL insertion, PCL insertion, and the inner part of the lateral condyle that extended to the junctional zone between Gerdy's tubercle and the tibial tubercle. The densest frequency of fracture lines in the above three areas was 131 out of 766. Moreover, cold zones were scattered in the posteromedial fragment, superior tibiofibular syndesmosis, Gerdy's tubercle, and tibial tubercle.

Axial view. In the lateral articular surface, the fracture lines were concentrated on the inner part and ran from the anterior to posterior direction, with the equator dividing the lateral surface into two halves. In the intermediate column without cartilage coverage, the fracture lines

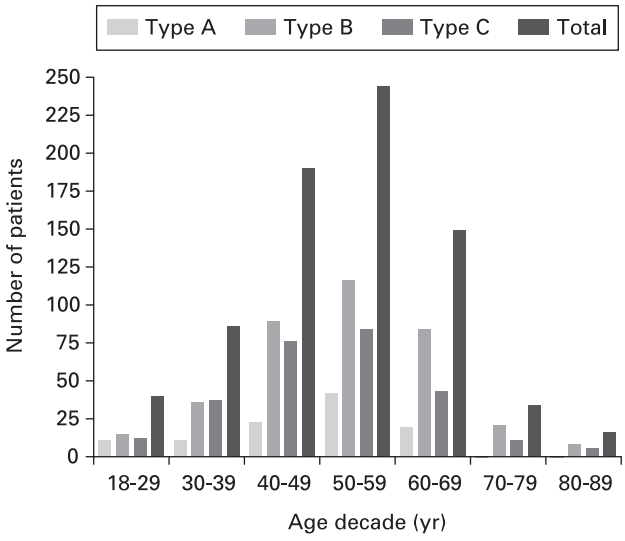

Fig. 2

The distribution of fractures by patient age and Orthopaedic Trauma Association/AO Foundation (OTA/AO) type.

were concentrated around the ACL and PCL insertion sites. The bare area was less involved, and the tibial tubercle area was a cold zone. The fracture lines in the medial articular surface were less concentrated, and fracture lines were as noted only through the middle and anteromedial area. The posteromedial fracture fragments were relatively intact (Figure 3f).

Surrounding view. In the anterior view, the fracture lines were concentrated on the junctional zone between Gerdy's tubercle and the tibial tubercle. Another minor fracture line originated from the lateral surface and exited inferior to the anteromedial cortex through the bare area (Figure 3g). In the posterior view, the PCL insertion area was a hot zone, whereas the posteromedial fragment and superior tibiofibular syndesmosis were clearly cold zones (Figure 3h). In the medial view, one major fracture line was observed, running in an anterosuperior to posteroinferior direction. Another main fracture line was noted in the middle area and divided the medial plateau into anterior and posterior parts (Figure 3i). In the lateral view, the fracture line was concentrated between the superior tibiofibular syndesmosis and Gerdy's tubercle and divided the lateral plateau into two parts (Figure 3j).

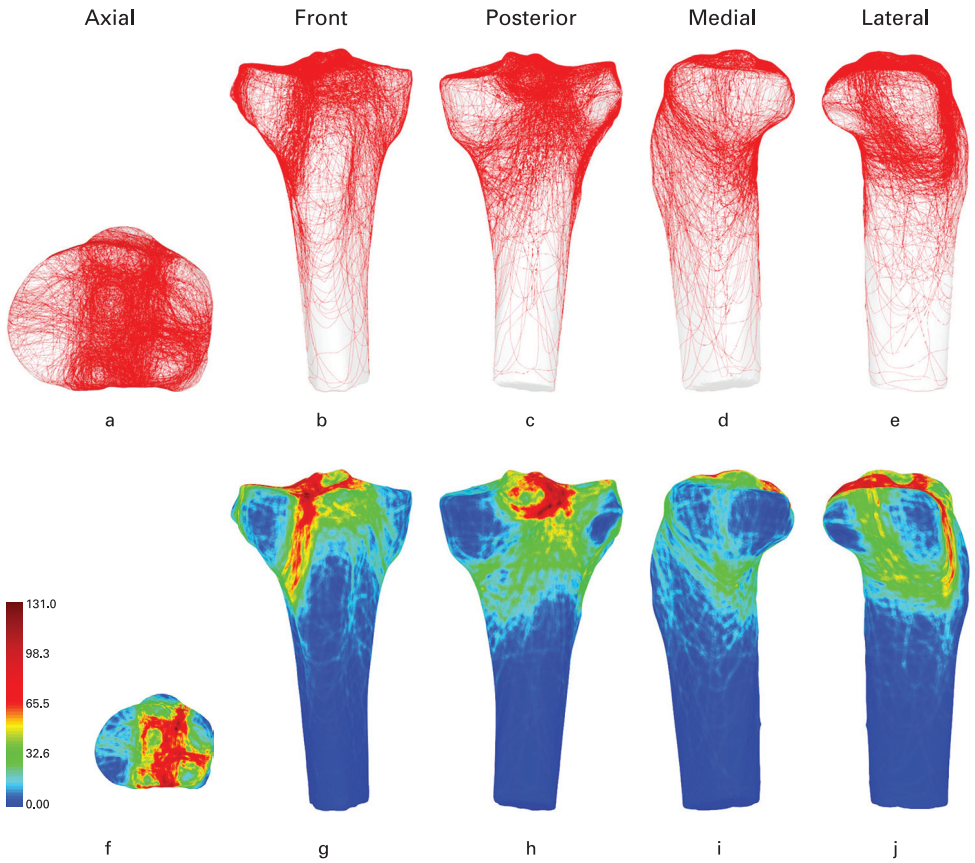

Fig. 3

a) to e) Representative views of the tibia template. f) to j) 3D heat mapping superimposed with all Orthopaedic Trauma Association/AO Foundation (OTA/AO) type A to C tibial plateau fracture lines (n = 766), including the axial, front, posterior, medial, and lateral views. Red colour represents a higher frequency of fracture line density.

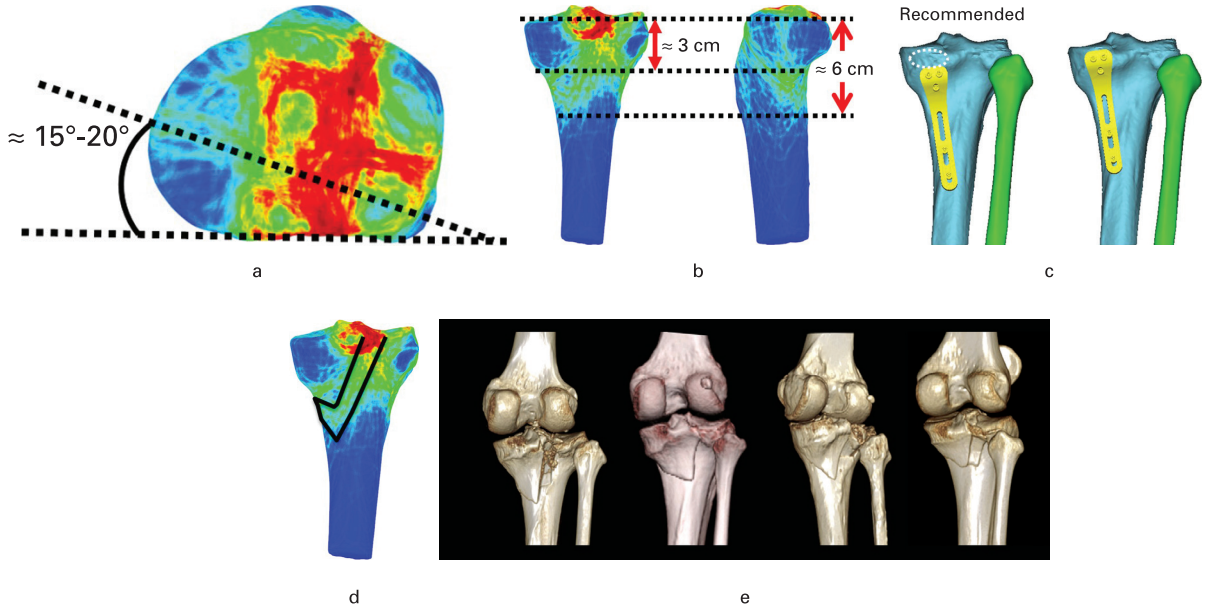

Fig. 4

a) Fracture angle between the line of posteromedial fragment and the posterior condylar axis was approximately 15° to 20° in the axis view. b) The distance from the articular surface was approximately 3 cm to the fracture line compact area and 6 cm to the acute vertex. c) The recommended location of the posteromedial plate. The white circle represents the insertion of the semimembranosus. d) Fracture line band, 'spur' sign indicated the presence of a classic flexion injury, as shown by the black line. e) Specific cases of the 'spur' sign.

With regard to the particular posteromedial fragment, the mean angle between the fracture line and the posterior tibial condylar was approximately 15° to 20° in the axis view (Figure 4a). The distance from the articular surface was approximately 3 cm to the fracture line compact area and 6 cm to the acute vertex (Figure 4b). There was an obvious fracture line band for the inferior border of the posteromedial fragment. The band originated from the border of the PCL fovea and posterolateral margin, obliquely extended to the tibial shaft, and sharply reversed to the medial plateau ('spur' sign; Figure 4d), thus indicating the presence of a classic flexion injury (Figure 4e).[24]

Moreover, the fracture lines for OTA/AO type A were mainly scattered around the AC and PCL insertion and the anterolateral ligament insertion (Segond fracture), with minimal involvement of the articular surface. The densest frequency of the fracture lines around the PCL insertion was 40 out of 114 (Figures 5a to 5e; Supplementary Video 2). In OTA/AO type B cases, the fracture lines were mostly concentrated on the lateral and intercondylar eminence. The tibial tubercle, tibial shaft, and medial column were rarely involved, except for the anteromedial margin. The densest frequency of fracture lines located in the inner border and equator of the lateral condyle was 71 out of 376 (Figures 5f to 5j; Supplementary Video 3). In OTA/AO type C cases, the fracture lines were distributed more widely and intricately, and involved the lateral, intermediate, and medial columns, as well as the tibial shaft. The densest frequency of the fracture lines located in the inner border of the lateral condyle and ACL and PCL insertion was 66 out of 276 (Figures 5k to 5o; Supplementary Video 4).

Discussion

In the present study, we used the 3D heat mapping technique to summarize the distribution and frequency of fracture lines for a large number of TPFs.

The overall heat mapping of TPFs showed that the distribution of fracture lines was not only dependent on the injury energy or mechanism, but was also distinctly related to the anatomical features of the proximal tibial area. Hot zones were observed around the intercondylar eminence (ACL and PCL insertion), whereas cold zones were noted around the superior tibiofibular syndesmosis (insertion of the fibular head ligament), Gerdy's tubercle (insertion of the iliotibial band (ITB)), tibial tubercle (PL insertion), and posteromedial fragment (attachment of the semimembranosus tendon or posterior medial corner) (Figure 6a). All the above distinctive bony areas were attached by crucial and strong ligaments or tendons. We believe that TPF fracture lines occur frequently in the transition zone with marked changes in cortical thickness. The intra-articular fracture lines were usually concentrated on the transition zone between the articular cartilage and the ligament insertion site, whereas extra-articular fracture lines were distributed in the transition zone of the metaphysis and diaphysis, similar to the fracture of the distal radii and surgical neck of the humeri. Moreover, the changes of bone microarchitecture will also affect the prone area of the fracture line.

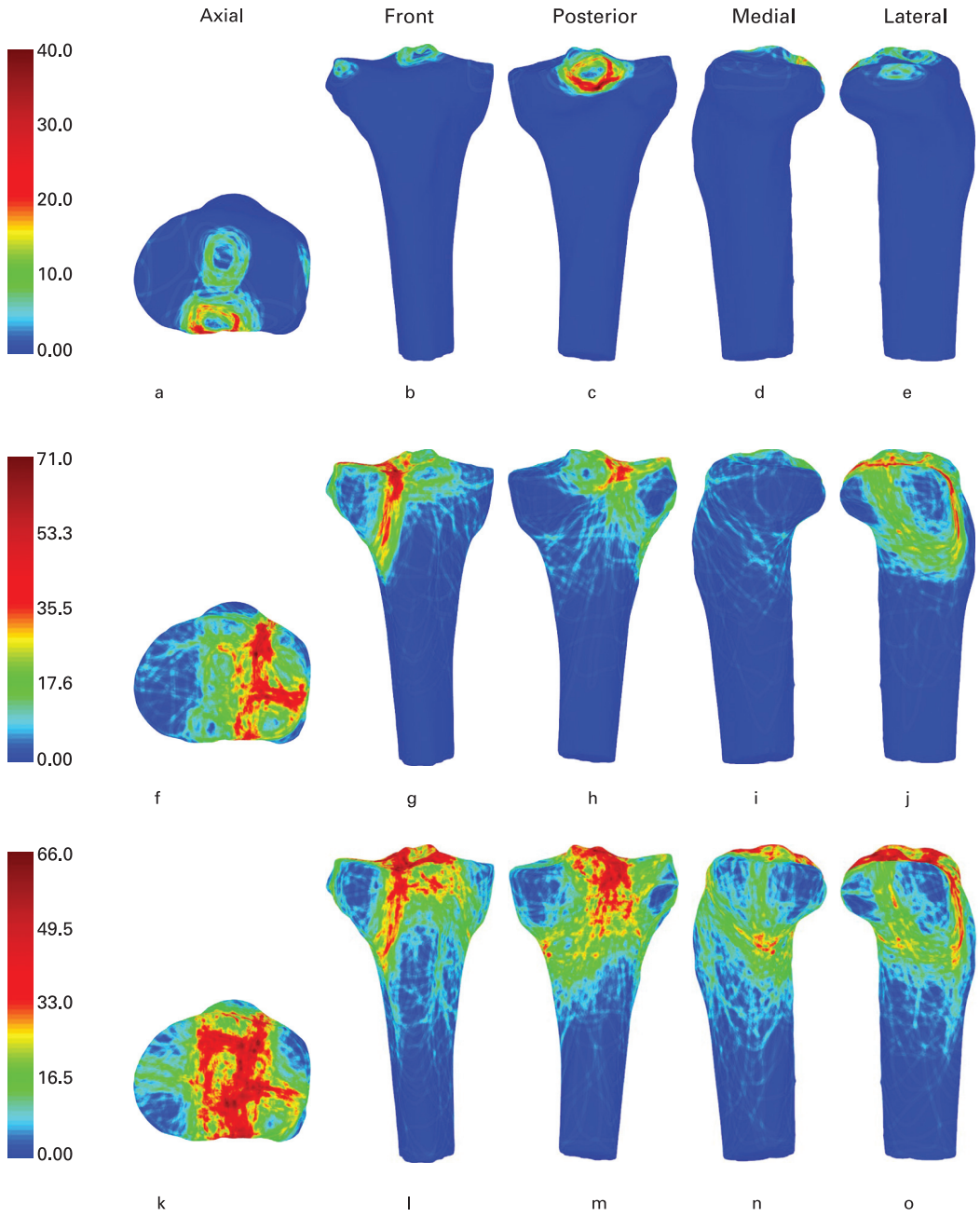

Fig. 5

Representative views of the 3D heat mapping of fracture lines according to the Orthopaedic Trauma Association/AO Foundation (OTA/AO): a) to e) type A; f) to j) type B; and k) to o) type C. These include the axial, front, posterior, medial, and lateral views. Red colour represents higher frequency of fracture line density.

In the axial plane, almost all classifications based on CT simply divided the upper surface of the tibial plateau into anterior and posterior halves, but no consensus was reached about the delimitation of the segment/column. The summarizing heat map showed a frequently occurring fracture line in the cartilage-covered area in both the lateral and medial condyles. The trajectory extended from the anteromedial to the posterolateral site (anterior rim of the fibular head; Figure 6a). In the three-column concept, the outer division was consistent with the trajectory, whereas the medial division (mirror image of the lateral line) was inconsistent with the heat map (Figure 6b). The horizontal line established by the eight-, ten-, and nine-segment classifications was also inconsistent with the inclined fracture line trajectory (Figures 6c to 6e).[12-14] Recently, the OTA/AO 2018, Yao 2018 , and Schatzker 2018 classifications designed the virtual equator according to the fibula head and medial collateral ligament, similar to the trajectory observed in the map (Fig. 6).[15-17]

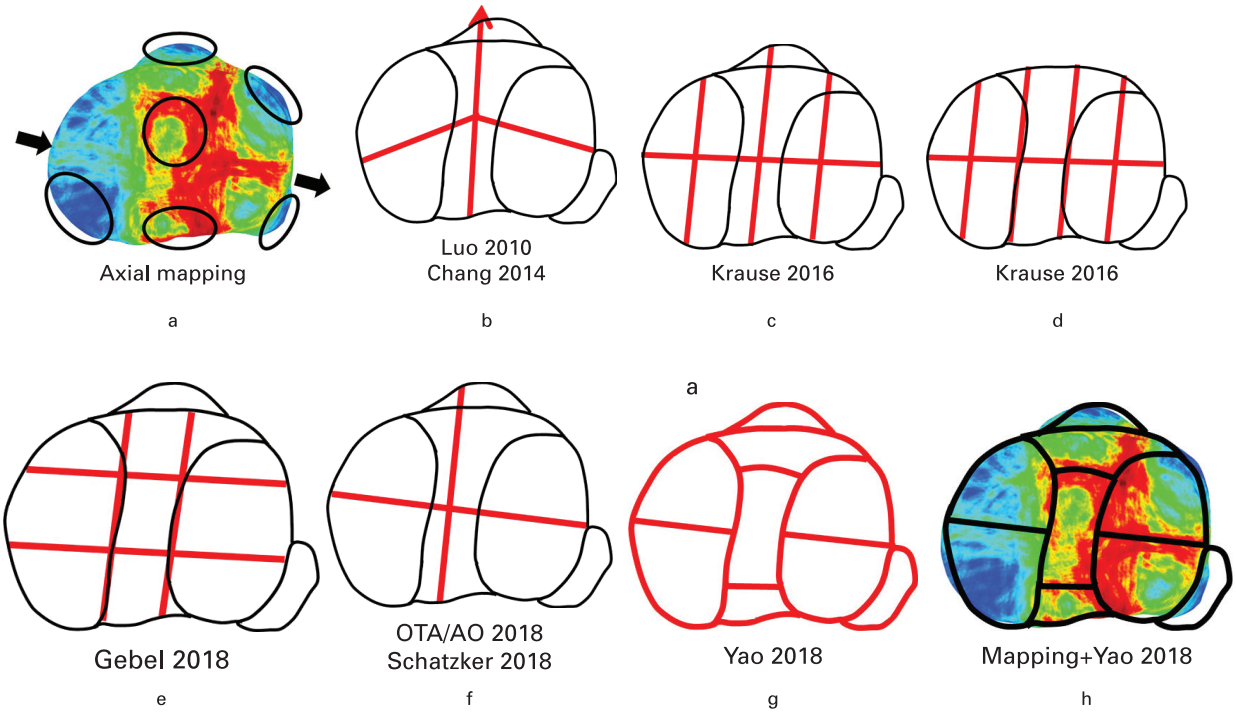

Fig. 6

Comparison of multiple classifications according to the heat mapping in the axial plane. a) Axial mapping. The black arrow shows the trajectory extended from the anteromedial to the posterolateral site. b) Three-column concept and four quadrants. c) Eight segments. d) Ten segments. e) Nine segments. f) Orthopaedic Trauma Association/AO Foundation (OTA/AO) 2018 and Schatzker 2018. g)[17] h) Axial mapping and Yao 2018.

The newly designated intermedial column without cartilage coverage—usually involving the tibial tubercle fragment and zone of comminution including the tibial spine—should not be ignored, given the high incidence of 74.9% (574 out of 766 knees).[13,21,25] The Schatzker and Luo classifications did not emphasize the intermedial column injury.[7,9,26] The OTA/AO 2018 classification recorded the isolated avulsion fracture of the tibial tubercle and tibial spine as 41A1.2 and 41A1.3 (Qualifications: o, anterior; p, posterior), which were neglected in more complex type B and C TPF cases.[16] The nine- and ten-segment classifications only calculated the fracture frequency of the intercondylar region.[13,14] The overall heat mapping indicated a hot zone around the ACL insertion in 358 cases (46.7%) and around the PCL insertion in 399 cases (52.1%), a moderate zone in the bare area in 304 cases (39.7%), and a cold zone in the tibial tubercle in 91 cases (11.9%). This finding was consistent with the values estimated in previous reports.[12,13,16,17] The marked difference in these four areas (Figure 6g: segments c, d, e, and f) supports the subdivision of the intermedial column in the Yao classification, which highlighted three ligament insertions crucial for knee stability and bony area indicating hyperextension TPF.[17]

In addition to the upper surface, the 3D heat mapping provided stereoscopic information about the extra-articular cortex. The surrounding maps indicated that the fracture lines generated from the lateral articular surface were obviously greater than those from the medial articular surface, consistent with previous studies.[13,14,17,22] In the front and posterior views, the fracture lines intricately extended along the metaphysis or diaphysis, despite having an origin at the upper surface. In the Schatzker classification, types I and II indicate the disruption of the lateral cortex, type IV describes the rupture of the medial cortex, and type V indicates bilateral condyle injury.[7,26] The OTA/AO 2018 classification added two qualifications (f, lateral; h, medial) to roughly describe cortex disruption.[16] However, the above classifications failed to depict the two special fracture lines that extended from the lateral cartilage facet to the medial cortex (Wahlquist Type C)[27] and from the medial cartilage facet to the lateral cortex.[28] The Yao classification established types 3 to 6 (homolateral/diaphyseal/contralateral/bilateral), and accordingly covered all injury types of the lateral and medial column. Hence, it was more comprehensive and beneficial for the determination of plate positioning.[29]

Furthermore, the fracture lines of the OTA/AO type B cases were mostly concentrated above the lower edge of the tibial tubercle, which usually extended beyond the tibial tubercle and involved the shaft in the OTA/AO type C cases (Figure 5). This finding suggests that more and longer plates should be prepared to fix type C TPFs.

The posteromedial fragment is relatively large and constant, and usually the first to be fixed as a reduction reference. Both clinical experience and biomechanical evidence support the fixation of the posteromedial fragment for inherent instability.[30-32] Mapping showed that

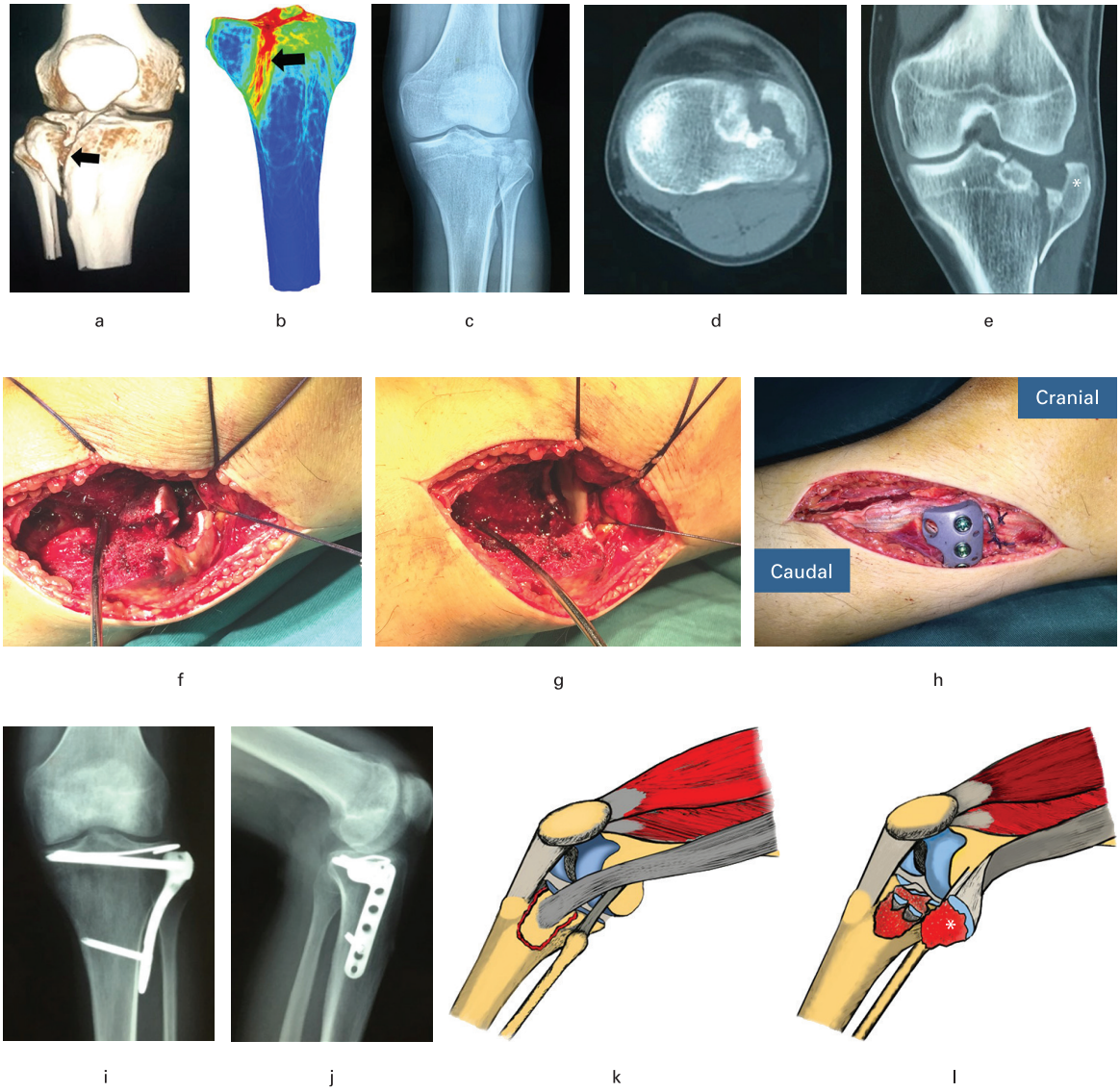

Fig. 7

The articular surface was reduced through the fracture gap, preserving the bone-tendon interface between the iliotibial band (ITB) and Gerdy's tubercle.
a) and b) The hot zone of fracture lines passing Gerdy's tubercle and the bare area/tibial tubercle. The black arrow represents the trajectory.
c) Preoperative radiograph. d) and e) Preoperative CT scans. f) and g) Exposure and reduction through the fracture gap. h) The insertion of the ITB was intact after the plate placement. i) and j) Postoperative radiographs. k) and l) The illustrations display the extorsion of Gerdy's tubercle fragment with the ITB. *The Gerdy's tubercle fragment.

the angle between the main fracture line and posterior bicondylar tibial plateau fracture was approximately 15° to 20°, consistent with the best fit line in previous studies.[21,33-35] Due to the attachment of posterior medial corner structure, the fracture line was approximately 3 cm to 6 cm below the articular surface in the postero-medial view (Figure 4b). Therefore, it was unnecessary to place the plates closely to the joint margin, as excessive exposure of posteromedial corner will inevitably disturb the posteromedial stability (Figure 4c). When the TPFs involved the posteromedial fragment, PCL insertion, and posterolateral compression, the posterior inverted L-shaped approach was recommended for addressing these three common posterior injuries.[36-38]

Another interesting finding was the hot zone of fracture lines passing Gerdy's tubercle and the bare area/tibial tubercle in the front view (Figures 7a to 7b). This high-incidence fracture line trajectory offers a ready-made intra-articular osteotomy of the lateral condyle through the anterolateral approach.[39-41] Figure 7 shows that the extorsion of Gerdy's tubercle fragment with the ITB can provide a clear surgical field for reduction, instead of the extensive detachment. The maintenance of the bone-tendon interface between the ITB and Gerdy's tubercle is essential to postoperatively reducing the anterolateral instability.[39,42]

This retrospective study has certain limitations. First, patients with no or insufficient CT data were excluded.

The exclusion of these patients led to statistical errors in the determination of the incidence rate, especially in OTA/AO type A fractures recognizable in radiograph. Second, due to the virtual reduction procedure, existing mapping technique can only show the distribution of the fracture line on the tibial surface, rather than the displacement and compression of the fragments. More innovative and injury mechanism-based imaging techniques are needed to implement relevant research.[43] Lastly, the influence of the mapping on the fixation scheme and clinical outcome required further discussion.

In conclusion, TPFs occurred more frequently in the lateral and intermedial column than in the medial column. Fracture lines of the tibial plateau occur frequently in the transition zone with marked changes in cortical thickness. According to the 3D heat mapping, the four-column and nine-segment classification had a high degree of matching as compared to the frequently used classifications.

Supplementary material

Videos showing the 3D heat mapping of all 766 tibial plateau fractures, as well as 3D heat mapping of tibial plateau fractures with Orthopaedic Trauma Association/AO Foundation (OTA/AO) types A, B, and C.

References

1. **Gaston P**, **Will EM**, **Keating JF**. Recovery of knee function following fracture of the tibial plateau. *J Bone Joint Surg Br*. 2005;87-B(9):1233–1236.
2. **Elsoe R**, **Johansen MB**, **Larsen P**. Tibial plateau fractures are associated with a long-lasting increased risk of total knee arthroplasty a matched cohort study of 7,950 tibial plateau fractures. *Osteoarthritis Cartilage*. 2019;27(5):805–809.
3. **Meulenkamp B**, **Martin R**, **Desy NM**, **et al**. Incidence, Risk Factors, and Location of Articular Malreductions of the Tibial Plateau. *J Orthop Trauma*. 2017;31(3):146–150.
4. **Millar SC**, **Arnold JB**, **Thewlis D**, **Fraysse F**, **Solomon LB**. A systematic literature review of tibial plateau fractures: what classifications are used and how reliable and useful are they? *Injury*. 2018;49(3):473–490.
5. **Hohl M**. Tibial condylar fractures. *J Bone Joint Surg Am*. 1967;49-A(7):1455–1467.
6. **Moore TM**. Fracture—dislocation of the knee. *Clin Orthop Relat Res*. 1981;156:128–140.
7. **Schatzker J**. Compression in the surgical treatment of fractures of the tibia. *Clin Orthop Relat Res*. 1974;105:220–239.
8. **Marsh JL**, **Slongo TF**, **Agel J**, **et al**. Fracture and dislocation classification compendium - 2007: orthopaedic Trauma Association classification, database and outcomes committee. *J Orthop Trauma*. 2007;21(10 Suppl):S1–S133.
9. **Luo CF**, **Sun H**, **Zhang B**, **Zeng BF**. Three-column fixation for complex tibial plateau fractures. *J Orthop Trauma*. 2010;24(11):683–692.
10. **Chang SM**, **Zhang YQ**, **Yao MW**, **et al**. Schatzker type IV medial tibial plateau fractures: a computed tomography-based morphological subclassification. *Orthopedics*. 2014;37(8):e699–e706.
11. **Wang Y**, **Luo C**, **Zhu Y**, **et al**. Updated Three-Column Concept in surgical treatment for tibial plateau fractures - A prospective cohort study of 287 patients. *Injury*. 2016;47(7):1488–1496.
12. **Krause M**, **Preiss A**, **Meenen NM**, **Madert J**, **Frosch KH**. 'Fracturoscopy' is superior to fluoroscopy in the articular reconstruction of complex tibial plateau fractures - an arthroscopy assisted fracture reduction technique. *J Orthop Trauma*. 2016;30(8):437–444.
13. **Krause M**, **Preiss A**, **Müller G**, **et al**. Intra-articular tibial plateau fracture characteristics according to the "Ten segment classification". *Injury*. 2016;47(11):2551–2557.
14. **Gebel PJ**, **Tryzna M**, **Beck T**, **Wilhelm B**. Tibial plateau fractures: fracture patterns and computed tomography evaluation of tibial plateau fractures in winter sports. *Orthop Rev (Pavia)*. 2018;10(1):7517.
15. **Kfuri M**, **Schatzker J**. Revisiting the Schatzker classification of tibial plateau fractures. *Injury*. 2018;49(12):2252–2263.
16. **Meinberg EG**, **Agel J**, **Roberts CS**, **Karam MD**, **Kellam JF**. Fracture and Dislocation Classification Compendium-2018. *J Orthop Trauma*. 2018;32(Suppl 1):S1–S170.
17. **Yao X**, **Xu Y**, **Yuan J**, **et al**. Classification of tibia plateau fracture according to the "four-column and nine-segment". *Injury*. 2018;49(12):2275–2283.
18. **Armitage BM**, **Wijdicks CA**, **Tarkin IS**, **et al**. Mapping of scapular fractures with three-dimensional computed tomography. *J Bone Joint Surg Am*. 2009;91-A(9):2222–2228.
19. **Cole PA**, **Mehrle RK**, **Bhandari M**, **Zlowodzki M**. The pilon map: fracture lines and comminution zones in OTA/AO type 43C3 pilon fractures. *J Orthop Trauma*. 2013;27(7):e152–e156.
20. **Xie X**, **Zhan Y**, **Dong M**, **et al**. Two and Three-Dimensional CT Mapping of Hoffa Fractures. *J Bone Joint Surg Am*. 2017;99-A(21):1866–1874.
21. **Molenaars RJ**, **Mellema JJ**, **Doornberg JN**, **Kloen P**. Tibial Plateau Fracture Characteristics: Computed Tomography Mapping of Lateral, Medial, and Bicondylar Fractures. *J Bone Joint Surg Am*. 2015;97-A(18):1512–1520.
22. **Chen P**, **Shen H**, **Wang W**, **et al**. The morphological features of different Schatzker types of tibial plateau fractures: a three-dimensional computed tomography study. *J Orthop Surg Res*. 2016;11(1):94.
23. **Xie X**, **Zhan Y**, **Wang Y**, **et al**. Comparative analysis of Mechanism-Associated 3-dimensional tibial plateau fracture patterns. *J Bone Joint Surg Am*. 2019. [Epub ahead of print] PMID: 31855868.
24. **Potocnik P**, **Acklin YP**, **Sommer C**. Operative strategy in postero-medial fracture-dislocation of the proximal tibia. *Injury*. 2011;42(10):1060–1065.
25. **Weil YA**, **Gardner MJ**, **Boraiah S**, **Helfet DL**, **Lorich DG**. Posteromedial supine approach for reduction and fixation of medial and bicondylar tibial plateau fractures. *J Orthop Trauma*. 2008;22(5):357–362.
26. **Schatzker J**, **McBroom R**, **Bruce D**. The tibial plateau fracture. The Toronto experience 1968—1975. *Clin Orthop Relat Res*. 1979;138:94–104.
27. **Wahlquist M**, **Iaguilli N**, **Ebraheim N**, **Levine J**. Medial tibial plateau fractures: a new classification system. *J Trauma*. 2007;63(6):1418–1421.
28. **Yeoh T**, **Iliopoulos E**, **Trompeter A**. An unclassified tibial plateau fracture: reverse Schatzker type IV. *Chin J Traumatol*. 2018;21(4):211–215.
29. **Zhang X**, **Lv B**, **Yao X**. Response to "Comments on: classification of tibial plateau fracture according to the 'four-column and nine-segment". *Injury*. 2020;51(2):577–578.
30. **Cuéllar VG**, **Martinez D**, **Immerman I**, **et al**. A Biomechanical Study of Posteromedial Tibial Plateau Fracture Stability: Do They All Require Fixation? *J Orthop Trauma*. 2015;29(7):325–330.
31. **Weaver MJ**, **Harris MB**, **Strom AC**, **et al**. Fracture pattern and fixation type related to loss of reduction in bicondylar tibial plateau fractures. *Injury*. 2012;43(6):864–869.
32. **Cherney S**, **Gardner MJ**. Bicondylar tibial plateau fractures: assessing and treating the medial fragment. *J Knee Surg*. 2014;27(1):39–45.
33. **Higgins TF**, **Kemper D**, **Klatt J**. Incidence and morphology of the posteromedial fragment in bicondylar tibial plateau fractures. *J Orthop Trauma*. 2009;23(1):45–51.
34. **Zhai Q**, **Hu C**, **Xu Y**, **Wang D**, **Luo C**. Morphologic study of posterior articular depression in Schatzker IV fractures. *Orthopedics*. 2015;38(2):e124–e128.
35. **Molenaars RJ**, **Solomon LB**, **Doornberg JN**. Articular coronal fracture angle of posteromedial tibial plateau fragments: A computed tomography fracture mapping study. *Injury*. 2019;50(2):489–496.
36. **Burks RT**, **Schaffer JJ**. A simplified approach to the tibial attachment of the posterior cruciate ligament. *Clin Orthop Relat Res*. 1990;254:216–219.
37. **Berber R**, **Lewis CP**, **Copas D**, **Forward DP**, **Moran CG**. Postero-medial approach for complex tibial plateau injuries with a postero-medial or postero-lateral shear fragment. *Injury*. 2014;45(4):757–765.
38. **Kołodziejczyk K**, **Kuliński K**, **Fedorowicz K**, **et al**. Difficulties in Treating Complex Knee Injuries with Fracture of Posterior Tibial Plateau. *Ortop Traumatol Rehabil*. 2018;20(4):293–300.
39. **Johnson EE**, **Timon S**, **Osuji C**. Surgical technique: Tscherne-Johnson extensile approach for tibial plateau fractures. *Clin Orthop Relat Res*. 2013;471(9):2760–2767.
40. **Sun DH**, **Zhao Y**, **Zhang JT**, **Zhu D**, **Qi BC**. Anterolateral tibial plateau osteotomy as a new approach for the treatment of posterolateral tibial plateau fracture: a case report. *Medicine (Baltimore)*. 2018;97(3):e9669.
41. **Hoekstra H**, **Vanhees J**, **van den Berg J**, **Nijs S**. Extended lateral column tibial plateau fractures. How do we do it? *Injury*. 2018;49(10):1878–1885.

42. Musahl V, **Herbst E**, **Burnham JM**, **Fu FH**. The anterolateral complex and anterolateral ligament of the knee. *J Am Acad Orthop Surg*. 2018;26(8):261–267.

43. Zhang BB, **Sun H**, **Zhan Y**, **et al**. Reliability and repeatability of tibial plateau fracture assessment with an injury mechanism-based concept. *Bone Joint Res*. 2019;8(8):357–366.

Author information:
- X. Yao, PhD, Associate Senior Doctor
- B. Lv, MD, Resident Doctor
- L. Wang, PhD, Associate Senior Doctor
- J. Xie, MD, Senior Doctor
- J. Yuan, PhD, Senior Doctor

Department of Orthopaedics, The Affiliated People's Hospital of Jiangsu University, Zhenjiang, China.
- K. Zhou, MD, Associate Senior Doctor, Doctor, Department of Orthopaedics, Qingpu Branch of Zhongshan Hospital, Fudan University, Shanghai, China; Department of Orthopaedics, the First Affilated Hospital of Soochow University, Soochow, China.
- X. Fu, MD, Senior Inspector, Jiangsu University Health Science Center, Zhenjiang, China.
- Y. Zhang, PhD, Attending Doctor, Department of Orthopaedics, Tongji Hospital, Tongji University School of Medicine, Shanghai, China.

Author contributions:
- X. Yao: Wrote the original draft of the manuscript, Performed the methodology, Acquired the funding.
- K. Zhou: Wrote, edited, and reviewed the manuscript.
- B. Lv: Curated the data.
- L. Wang: Performed the investigation.
- J. Xie: Carried out the project administration.
- X. Fu: Performed the visualization.
- J: Yuan: Conceptualized the study.
- Y. Zhang: Acquired the software and funding.

Funding statement:
- No benefits in any form have been received or will be received from a commercial party related directly or indirectly to the subject of this article.

ICMJE COI statement:
- X. Yao reports institutional grants (paid to The Affiliated People's Hospital of Jiangsu University) from the Zhenjiang Science & Technology Program (Grant Number: SH2017029), Clinical Medical Science and Technology Development Foundation of Jiangsu University (Grant Number: JLY20180043), and 333 plan of Jiangsu province (Grant No: to be confirmed), all related to this study. Y. Zhang reports institutional grants (paid to Tongji University School of Medicine) from the Shanghai Municipal Commission of Health and Family Planning (Grant Numbers: 201740078 and 20184Y0279), all related to this study.

Acknowledgements:
- We thank Prof. Xirui Wu and Prof. Wenxiang Li for providing the case in Figure 7.
- Xiang Yao, Kaihua Zhou, and Bin Lv contributed equally to this work.

Ethical review statement:
- This retrospective study has been approved by the ethical committee of the Affiliated People's Hospital of Jiangsu University.